Two-dimensional granular flow in a vibrated small-angle funnel

K. Lindemann and P. Dimon
The Center for Chaos and Turbulence Studies, The Niels Bohr Institute, Blegdamsvej 17, DK-2100 Copenhagen Ø, Denmark
(Received 7 May 2000)

We have studied the flow of a single layer of uniform balls in a small-angle funnel when it is vibrated parallel to the flow. Generally, we measured the flow rate as a function of a dimensionless acceleration Γ. However, for sufficiently small outlet widths, the flow can jam so we also measured the elapsed times between balls and their correlations to study jam dynamics. In particular, we found that when the funnel angle β was larger than $\sim 4°$, a stable jam always formed for $\Gamma < 1$ and the flow stopped. For $\Gamma \sim 1-4$, jams still occurred, but now they broke and reformed, although they could last ~ 100 s, resulting in long-time correlations in the flow. The elapsed time distributions in this case show distinct, possibly algebraic, tails. Beyond $\Gamma \sim 4$, the flow no longer jammed and the flow rate became constant. The general behavior has been mapped out in a rough phase diagram.

PACS number(s): 45.70.Mg

I. INTRODUCTION

The flow properties of a single layer of uniform brass balls rolling down an inclined plane through a small-angle funnel have been studied by Veje and Dimon (VD) [1]. In effect, this was a two-dimensional analog of an hourglass, but with the capability to observe the flow in detail. In particular, it was found that the flow jammed for sufficiently small funnel outlet widths. We have constructed a smaller version of that experiment, and subjected it to vibrations parallel to the flow in order to study the dynamics of the jamming process [2]. Related experiments have been performed on a wide-angle hopper [3,4] and an hourglass [5] but for rather different parameter ranges. Consequently, the dynamics in those experiments (which will be discussed in Sec. VI) are distinctly different from those reported here.

The paper is structured as follows. We describe the experimental setup in Sec. II and the different types of measurements in Sec. III. We show our results for an unvibrated flow in Sec. IV. The properties of jams are discussed in Sec. V. In Sec. VI we present the flow rate measurements and the elapsed time measurements and their correlations for a vibrated flow. Finally, we summarize the salient points in Sec. VII.

II. EXPERIMENTAL SETUP

The granular material consisted of 10 000 brass balls of diameter $d = 3/32$ in. (≈ 2.38 mm) with a diameter deviation of $\pm 1\%$ and a sphericity of $\pm 0.2\%$. The average mass of a single ball was $m = 0.0594$ g. Brass balls were used to avoid the effects of magnetization. The coefficient of restitution of the balls was measured to have a lower bound of ~ 0.74.

A schematic of the experiment is shown in Fig. 1. A plexiglass plate (A) (40 cm long, 35 cm wide, 0.6 cm thick) was equipped with slides which glided on two fixed rails (B). The rails were mounted on a plastic box (C) which itself was mounted on a heavy aluminum plate (D) with adjustable feet (E). The plastic box was tilted at an angle $\theta = 4°$ from the horizontal as in VD. (This angle was found in VD to have little effect on the flow and was therefore fixed in the interest of stability.)

A funnel was made by placing two 2.5-mm-high aluminum walls (F) on the plexiglass plate (A). They had 28-cm-long straight sections which opened smoothly at the top to form a reservoir. The ratio of the funnel length to the ball diameter was therefore ~ 100 as compared with ~ 600 in VD, so this is not a fully scaled down version of that experiment. (This was necessary for practical reasons such as weight and expense.) The walls could be moved to vary both the funnel half-angle β from 0° to 7° and the outlet width D from 0 to 25 mm. They were positioned at the outlet using fixed-width calipers, so the uncertainty in D was ± 0.1 mm. The funnel width near the reservoir was measured with a ruler giving an uncertainty in β of $\pm 0.05°$. The walls were grounded to prevent the accumulation of static electricity. A plexiglass cover plate (G) was placed on top of the walls to keep the balls in a single layer. The balls were fed into the system through a funnel (H) attached to the top plate. After leaving the funnel, the balls rolled through a plastic tube (I) into a container (J). All surfaces were routinely cleaned with isopropanol. The balls were cleaned by washing them in a mild soap and water solution, then rinsing them with water followed by isopropanol.

The plate (A) was connected by a 19-cm camshaft (K) to a cam (L) driven by a 24-V dc motor (M). The cam was fitted with holes to allow six different vibration amplitudes, specifically 1, 2, 4, 6, 8, and 10 mm. The frequency of the motor could be varied continuously in the range 0.5–10 Hz by changing the supply voltage. (This reduces the motor's torque at low frequencies, but the advantages of using a dc motor in this manner outweighed the relatively minor disadvantages.) Hence, all measurements were made by fixing the amplitude and varying the frequency.

The total mass of the outflow in the container (J) was measured with a Sartorius PT 1500 scale (N) which had a range of 1500 g, a precision of 0.1 g (approximately two ball masses), and a relaxation time of ~ 1.5 s. (The additional force caused by the falling of balls into the container was roughly the weight of a single ball and hence could not be resolved.) The scale was interfaced to a computer which took

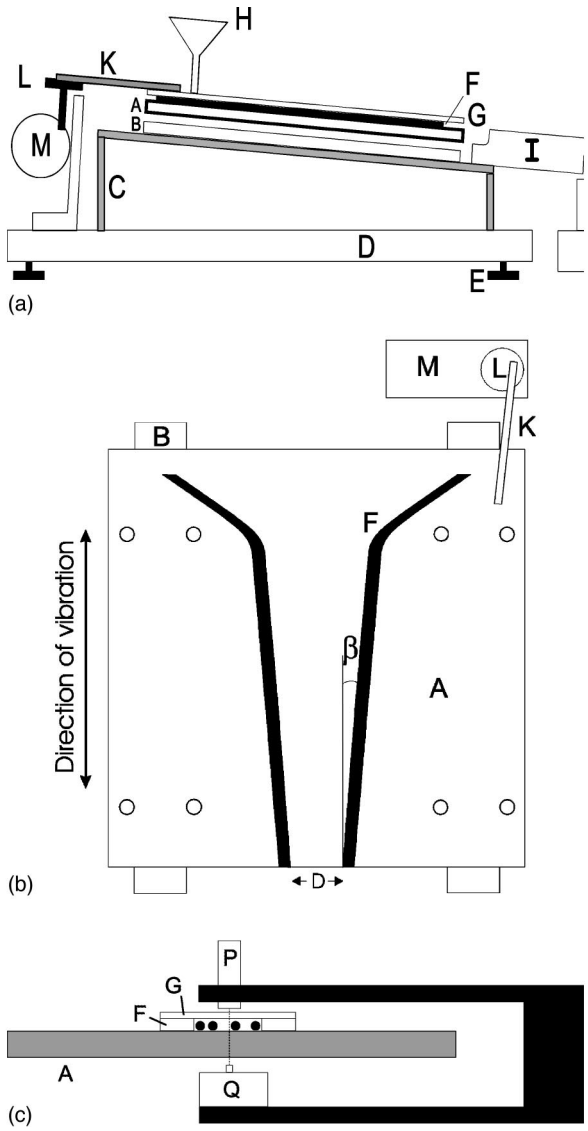

FIG. 1. The experimental setup: (a) side view, (b) top view, and (c) optical system.

readings at 5 Hz. To avoid transient effects, the balls were always allowed to flow for ~ 10 s before making any measurements. This also eliminated any memory effects, i.e., hysteresis, when any parameters were changed.

When the outlet width was so small such that only a single ball could pass through at a time (i.e., $D/d<2$), we also measured the elapsed times between balls with an optical detector which straddled the plexiglass plate (A) from the side. This consisted of a 670-nm laser diode (P) and a photodiode (Q) as shown in Fig. 1(c). The laser was focused in the plane of the balls to a spot less than 10% of the projected area of a ball so it was effectively a point measurement. This system was placed just below the outlet so that all balls leaving the funnel intersected the beam. A jam, therefore, could not block the beam. The signal from the photodiode was sampled at 500 Hz with an analog-to-digital converter card in the computer. The frequency response of the optical system was checked by modulating the laser and was found to be flat up to ~ 10 kHz.

The movement of the plate was monitored with a Brüel & Kjær type 4503 accelerometer whose signal was measured

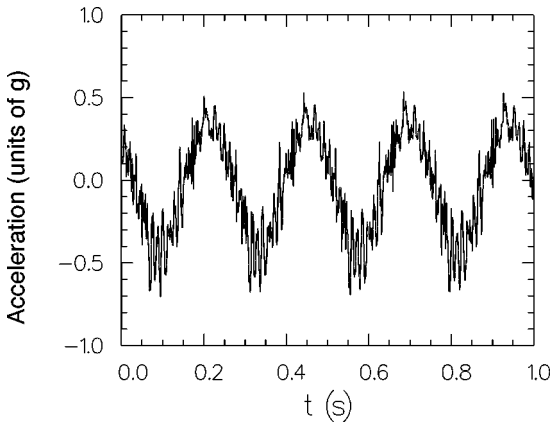

FIG. 2. The acceleration of the plate relative to gravity, sampled at 1024 Hz.

with an HP3562A Dynamic Signal Analyzer for harmonic content. The vibration frequency was determined to within ± 0.04 Hz from the power spectrum of this signal. (It was observed that the frequency of the motor drifted as it warmed up from a cold start, so the motor was run for at least half an hour before making any measurements until it stabilized.) The cam introduces harmonics into the position of the plate $x(t)$. To second order in the ratio $\epsilon = A/L_c$, where A is the vibration amplitude and L_c is the camshaft length, this is given by $x(t) \simeq L_c[1-\epsilon^2/4-\epsilon\cos\omega t+(\epsilon^2/4)\cos 2\omega t]$. For the largest vibration amplitude $A=10$ mm, the ratio of the amplitudes of the second harmonic to the first harmonic is therefore $\epsilon/4 \simeq 0.013$.

An example of the signal from the accelerometer is shown in Fig. 2. (No balls were in the system, but there was no significant change if otherwise.) It is essentially sinusoidal, but clearly there are higher frequencies present also. The power spectrum of a similar signal is shown in Fig. 3 when the driving frequency was 2.3 Hz and $A=10$ mm. The harmonic contamination of the acceleration is now apparent. The second harmonic is at least 100 times smaller than the first, hence the ratio of the *amplitudes* of the second to first harmonic of the *position* is ~ 0.025. Therefore, comparing with our estimate above, we see that roughly half of the second-harmonic contribution in the position is from the camshaft. The remaining harmonic contributions are due to mixing of the motor's commutator frequency.

As discussed in VD, the interstitial fluid does not play an

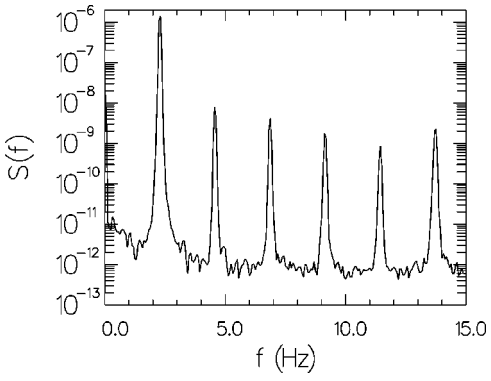

FIG. 3. Power spectrum of the plate acceleration showing the vibration frequency and its harmonics.

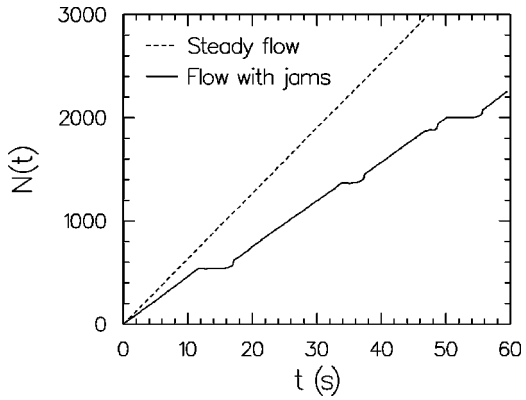

FIG. 4. Number of collected balls vs time for steady flow (dashed line) and flow with jams (solid line).

important role in the flow. The Bagnold number (which measures the relative importance of viscous drag to inertia) for balls moving at the maximum velocity $v_m \sim 30$ cm/s (i.e., rolling freely) is $\mathrm{Ba} = 3\pi\eta d v_m / m g' \sim 3 \times 10^{-3}$, where η is the dynamic viscosity of air, and $g' = g \sin\theta$ is the gravitational acceleration in the plane of the flow. Also, the Reynolds number in this case is $\mathrm{Re} = v_m d/\nu \sim 50$, where ν is the kinematic viscosity of air, whereas turbulence does not occur until $\mathrm{Re} \sim 200$.

III. MEASUREMENTS

For comparison with previous work, the total mass outflow measured by the scale was divided by the ball mass m to obtain the total number of collected balls $N(t)$. Figure 4 shows typical measurements of $N(t)$ for a vibrated system with two different configurations, one exhibiting a steady flow, i.e., one without any jams (dashed line), and the other a flow with jams (solid line). One can see that the latter alternates between a jammed state (horizontal regions) and a steady flow. The mean flow rate after a time T is simply $Q = N(T)/T$. It could also be obtained from the slope of linear fits to $N(t)$. The fitted values were consistent with Q, even when there were jams, indicating that $N(t)$ was, on average, linear. This implies that the jamming/unjamming process is stationary.

In the case of steady flow, the mean flow rate Q was generally reproducible. (The error of Q is obtained from the standard deviation of the distribution of the local value of dN/dt, accounting for the short-time correlations due to the relaxation time of the scale.) In the case of flow with jams, however, consecutive measurements often yielded wildly varying flow rates, depending on the duration of the jams. The statistics could not be improved by repeating the measurement. In fact, as we will see in Sec. VI D, the elapsed time distributions show that the jam durations have a divergent mean.

When $D/d < 2$, it is possible to detect each ball with the optical system. A short segment of the signal from the optical detector is shown in Fig. 5(a), where one can see the passing of ~ 10 balls. (The intensity fluctuations when the beam was unblocked were due to the imperfectly uniform transparent flow plane and top plate.) A threshold criterion (dashed line) determined the presence (or absence) of a ball

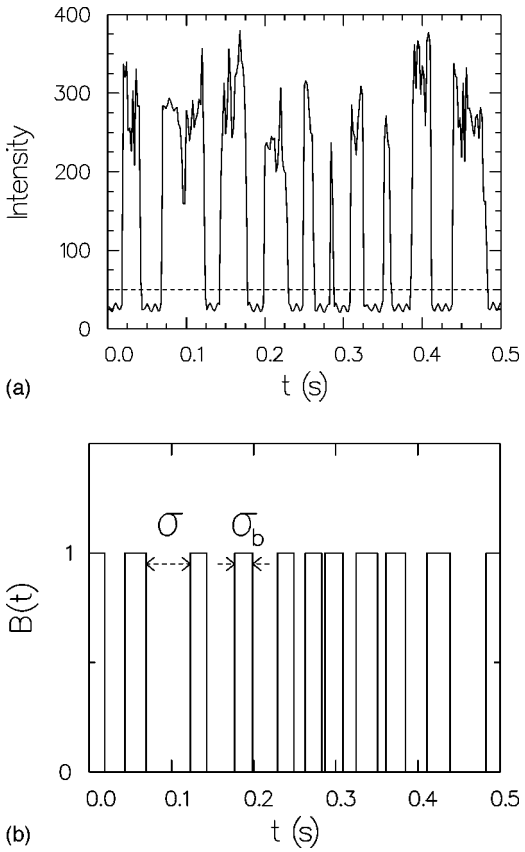

FIG. 5. (a) Photodiode output (light intensity) sampled at 500 Hz. A value close to zero indicates a ball is blocking the beam. The horizontal dashed line shows the threshold value used to decide whether a ball is in the beam or not. (b) The idealized binary signal $B(t)$ obtained by applying the threshold criterion. A value of 1 indicates a ball is blocking the beam. The elapsed time σ and blocked time σ_b were obtained from $B(t)$ as shown.

and was used to generate a purely binary signal $B(t)$. The idealized representation of $B(t)$ corresponding to Fig. 5(a) is shown in Fig. 5(b). The elapsed time σ and blocked time σ_b were then obtained from $B(t)$ as indicated in the figure. (The elapsed times were measured partly because it proved impossible to establish a robust criterion for defining a flowing or truly jammed state, although, as will be shown later in Sec. VI D 2, these states do manifest themselves in the elapsed time distributions.) Note that with a sampling rate of 500 Hz, the smallest measureable σ is 0.002 ± 0.001 s. For a typical ball velocity of 10 cm/s, this implies an effective spatial resolution of ~ 0.1 mm. Data were normally collected for 150 000 samples, or 300 s, hence the total number of detected balls depends on the flow rate.

Using a light chopper attached to the plate in conjunction with a lock-in amplifier, we also attempted to measure the phase shift between the motion of the plate and the signal from the optical system (which reflects the motion of the balls). No well-defined phase shift could be detected, although some correlations certainly exist (see Sec. VI D).

IV. UNVIBRATED FLOW

A. Qualitative behavior

First, we discuss the properties of an unvibrated flow. These have already been studied in greater detail in VD, but

we now summarize the results for comparison later. It was found in VD that for certain values of D/d in the range $D/d \sim 1-3$, the balls would jam near the outlet and the flow would stop. These jams are the primary interest of the present work and we will postpone a discussion of them until Sec. V. For $D/d > 3$, the flow no longer jammed and there were three different regimes as a function of the funnel half-angle β. For $D/d = 3.14$, they were as follows.

(i) $\beta < 0.05°$: Pipe flow. There was a nearly stationary shock wave about 20–30 cm below the reservoir, after which the balls mostly accelerated freely.

(ii) $\beta \sim 0.05° - 1°$: Intermittent flow. Kinematic shock waves propagated upstream, disturbing the flow. (These have been studied in detail in another work [6].)

(iii) $\beta > 1°$: Steady flow. The flow was of nearly uniform density (although weak shock waves could still be seen).

We repeated similar measurements with the present setup, although recall that this is not a rescaled version of the one in VD, so we should expect some differences. For $D = 8$ mm ($D/d = 3.36$), the following behavior was observed.

(i) $\beta < 0.5°$: Free flow. The balls just accelerated freely. The funnel was probably not long enough to allow the formation of the stationary shock observed in VD for pipe flow.

(ii) $\beta \sim 0.5° - 1.5°$: The behavior depended on the initial state. For an initially filled funnel, intermittent flow with shock waves was observed as in VD. For an initially empty funnel, free flow was observed. In both cases, the flow behavior remained stable during the measurement period.

(iii) $\beta > 1.5°$: Steady flow as in VD, with weak shock waves visible up to $\beta \sim 2.5°$.

B. Flow rate measurements

As in VD, we measured mean flow rates and compared them with the prediction of Brown [7,8] as modified in VD for rolling balls. For a small-angle funnel ($\beta \ll 1$) on a slightly inclined plane ($\theta \ll 1$), this can be written as

$$Q = (40/7)^{1/2} (C/\pi d^2) g^{1/2} D^{3/2} \beta^{-1/2} \theta^{1/2}, \qquad (1)$$

where the only unknown parameter is the two-dimensional packing fraction C [9]. For triangular close-packed spheres $C = \pi/2\sqrt{3} \approx 0.91$. (Note that in this work β is always below the angle of approach, which is known to be $\sim 15°$ [8].)

1. β dependence

Figure 6 shows the flow rate Q as a function of β for $D = 7$ mm ($D/d = 2.94$). It reaches a maximum at $\beta_p \sim 0.8°$ for the same reason discussed in VD, namely, the flow rate is governed by the outlet for $\beta > \beta_p$ and by the inlet from the reservoir for $\beta < \beta_p$. The peak position here is higher than the value $\beta_p \sim 0.3°$ found in VD, but it was argued in that work that the peak is essentially a finite-size effect and that $\beta_p \sim D/L$, where L is the length of the system. This would predict that in the present setup β_p ought to be $\sim 1.5°$, which is somewhat larger than observed. Generally, all flow regimes in the present work occurred at larger angles than in VD. Otherwise, the data were qualitatively the same.

In Fig. 6, the data for $\beta > \beta_p$, which should follow Eq. (1), are shown fitted with a power law yielding $Q \sim \beta^{0.42 \pm 0.02}$. The exponent is lower than the predicted value of $\frac{1}{2}$, but is consistent with the value found in VD. The inferred packing fraction was found to be $C = 0.56 \pm 0.03$, lower than expected for dense packing, though slightly larger than found in VD.

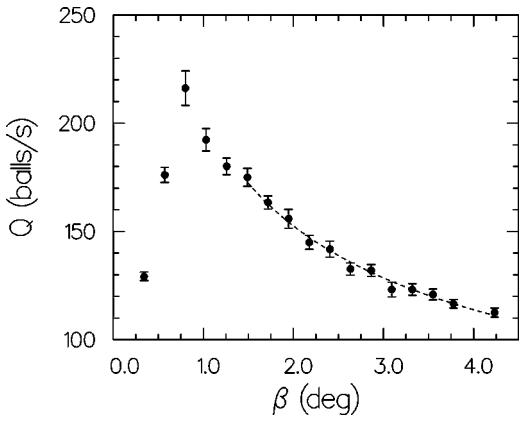

FIG. 6. Flow rate vs funnel angle for $D = 7$ mm ($D/d = 2.94$). The dashed line is a power-law fit (see text).

Flow rates were also measured for $D = 3$ mm ($D/d = 1.26$) and $D = 5$ mm ($D/d = 2.10$). If the flow rate Q is rescaled by a factor $D^{3/2}$, then these data should collapse in the region $\beta > \beta_p$ where Eq. (1) is valid. However, the peak positions will still not coincide. If $\beta_p \sim D/L$ as argued in VD, then $Q(\beta_p) \sim D^{3/2} \beta_p^{-1/2} \sim D L^{1/2}$. Thus, if one plots Q/D versus β/D, the data should collapse everywhere except in the free flow regime $\beta < \beta_p$. This rescaling is shown in Fig. 7. (For $D = 3$ mm the flow was constantly jamming for smaller β so a meaningful peak position could not be determined.)

2. D dependence

Figure 8 shows the flow rate Q as a function of D/d for two values of β in the steady flow regime. For $1 < D/d < 6$, one observes a reproducible steplike structure, also found in VD. (These steps were more distinct in VD, where it was possible to make finer adjustments in D.) In particular, note that there is a jammed state (i.e., $Q = 0$) for one measurement at $D/d \sim 1.5$. Power-law fits to these data sets (not shown for clarity) are sensitive to the steps, but yielded results in the range $Q \sim D^{1.4-1.6}$, consistent with Eq. (1), and

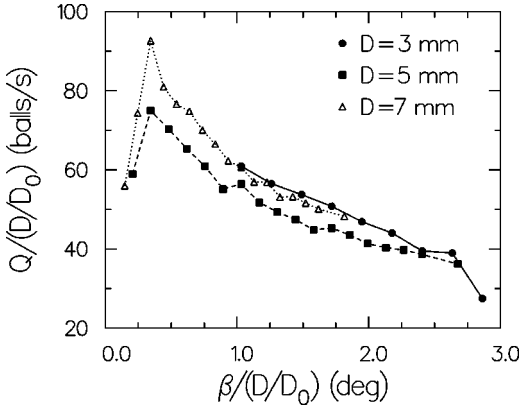

FIG. 7. Rescaled flow rate vs rescaled funnel angle with $D_0 = 3$ mm. Error bars are omitted for clarity. The connecting lines are guides to the eye.

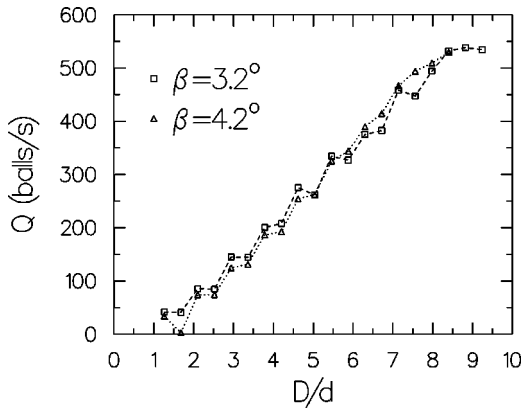

FIG. 8. Flow rate vs the ratio D/d for two different values of the funnel angle. Error bars are omitted for clarity. The connecting lines are guides to the eye.

again also with VD. The deduced packing fraction was in the range $C=0.4$–0.5, consistent with the result above for $Q(\beta)$.

V. JAMS

The primary purpose of this experiment was to study jams and the effect of vibrations on them. In an *unvibrated* system, they were observed to have the configurations shown schematically in Fig. 9. Most commonly, a jam occurred when two balls formed a small arch near the outlet as in Figs. 9(a) and 9(b). Jams involving three balls as in Fig. 9(c) were seen approximately five times during the entire experiment (roughly one year). Jams with more than three balls were never observed. For $\beta<0.5°$, jams consisting of four to five balls also occurred at the *inlet* to the funnel as shown schematically in Fig. 10.

In a *vibrated* system, only the two ball jams were observed. However, their relative stability depends strongly on the configuration. The jam in Fig. 9(a) usually occurred during steady flow when the flow was densest. When vibrated, it is not very stable since even a small perturbation will allow the ball closest to the outlet to fall out. The jam in Fig. 9(b) is much more stable than (a) for three reasons: (i) a much larger rearrangement is required to free one of the two balls closest to the outlet, (ii) during vibrations, the two balls tend to move up and down together, so the required rearrangement is not likely to occur, and (iii) the ball immediately above them stabilizes the situation even further.

VI. VIBRATED FLOW

When the system is vibrated, there are two additional parameters, the vibration frequency $\omega=2\pi f$ and amplitude A.

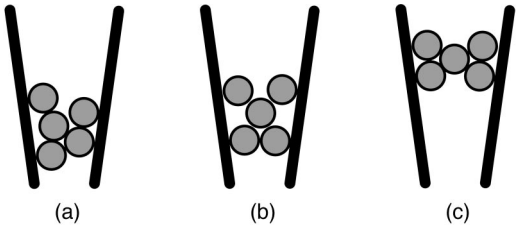

FIG. 9. Three different jam configurations near the outlet of the funnel (see text).

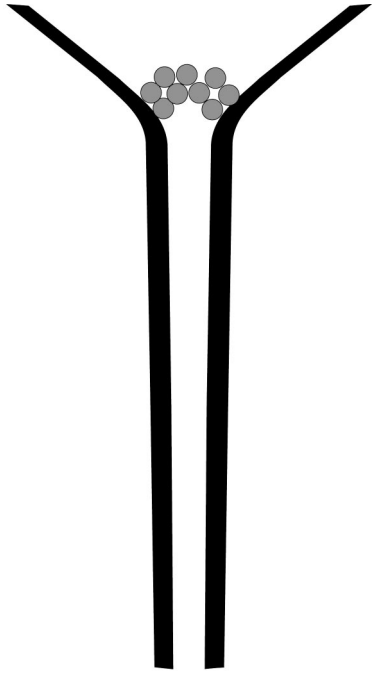

FIG. 10. A jam at the inlet of the funnel.

One commonly defines a dimensionless acceleration $\Gamma=A\omega^2/g'$ as a control parameter [10]. (Note that we use the gravitational acceleration in the plane of the flow $g'=g\sin\theta$.) For outlet-dominated flow, the flow rate always stabilized for sufficiently large Γ, although it was not always a function of Γ alone. Generally, Γ was always increased. (As stated earlier, all measurements were started from the flowing state, eliminating any hysteresis effects.)

We studied the behavior in the following parameter ranges:

$$D=3,4,\ \text{and}\ 5\ \text{mm}\quad (D/d=1.26,1.68,2.10),$$

$$\beta=0.1°,0.8°,2.0°,3.1°,4.2°,5.4°,\ \text{and}\ 6.5°,$$

$$f=0.5-10\ \text{Hz},$$

$$A=1,2,4,6,8,\ \text{and}\ 10\ \text{mm},$$

$$\Gamma=0-58.$$

Since the purpose of this work was primarily to study the effect of vibrations on a jammed state, we will concentrate on the measurements for $D=3$ mm ($D/d=1.26$) when jams for $\Gamma=0$ were observed to occur for some values of β. Jams were rarely observed for larger D, hence the effect of vibrations was not particularly dramatic, although not without interest. These data will be discussed later in Sec. VI C.

A. Qualitative behavior for $D=3$ mm ($D/d=1.26$)

The behavior of the flow has been summarized in a rough phase diagram Fig. 11. The horizontal boundaries separating the different phases as a function of β are only intended for clarity since we have insufficient data to locate them accurately. (Also, the flow does not necessarily depend on Γ alone.) We identify three new flow types associated with a

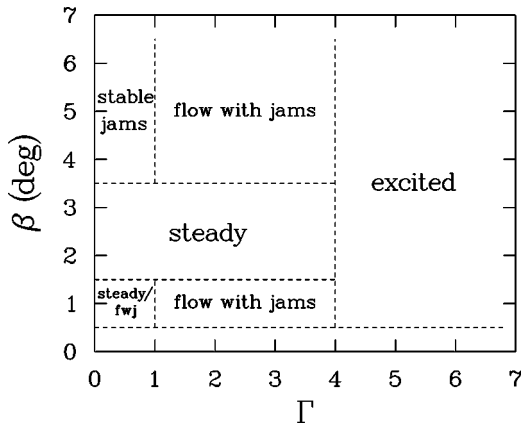

FIG. 11. Phase diagram showing the different flow types for $D=3$ mm ($D/d=1.26$). The boundaries (dashed lines) should only be taken as rough guides.

vibrated flow. In particular, all three types occur for $\beta \geqslant 4.2°$, where we note the following behavior with increasing Γ: (i) $\Gamma<1$: Stable jam. An apparently unbreakable jam always forms. (ii) $\Gamma\sim 1-4$: Flow with jams. The system alternates between a flowing state and a jammed state as in Fig. 4. (iii) $\Gamma>4$: Excited flow. The flow no longer jams. The balls near the outlet are always rather excited. In addition to these, a steady flow as discussed in Sec. IV A, i.e., a relatively dense flow without jams, also survived in the presence of vibrations for $\beta=2.0°$ and $\beta=3.1°$ and for $\Gamma<4$. We now discuss the new flow types in more detail.

1. Stable jams

Even when the system was vibrated, jams still occurred, but their duration depended strongly on Γ. For $\beta \geqslant 4.2°$, the jams remained stable until $\Gamma\sim 1$ (see Fig. 11). (Of course, in principle, one has to measure for an infinitely long time to determine whether a jam is truly stable or not. In general, these jams were observed for ~ 15 min before the measurement was stopped.) As might be expected, stable jams were virtually always of the type shown in Fig. 9(b).

2. Flow with jams

Jams still occur, but now they are of finite duration, decreasing in some cases from ~ 100 s to ~ 1 s with increasing Γ in 300-s runs. Longer runs of ~ 2 h were made for a few values of Γ to see if longer jams occurred, and indeed they did. Jam lifetimes will be discussed further in Sec. VI D. The flow was relatively steady between jams, as can be seen in Fig. 4.

3. Excited flow

Jams could not form when the system was strongly vibrated. Moreover, balls near the outlet tended to bounce violently off the walls and each other, hindering them from finding their way out of the funnel. This resulted in lower flow rates than for steady flow, although generally higher than for flow with jams. It also appeared to the eye that when one ball managed to escape, a group of two to five balls sometimes followed closely behind it, resulting in brief jumps in the flow rate. The density fluctuations at the outlet also tended to generate visible kinematic shock waves which propagated upstream.

B. Flow rates for $D=3$ mm ($D/d=1.26$)

The phase diagram Fig. 11 was measured for fixed β and increasing Γ. We now discuss the flow behavior and flow rate measurements as a function of β.

1. $\beta=0.1°$

The flow behavior in this range is entirely dominated by the dynamics at the *inlet* and hence is not really pertinent. Balls that enter the funnel just roll out freely. Figure 12(a) shows the flow rate Q for $\beta=0.1°$ and six different values of A. For $\Gamma=0$ only, inlet jams occur as discussed in Sec. V. When Γ is increased, there is flow with jams followed by excited flow, just as with outlet jams.

2. $\beta=0.8°$

Figure 12(b) shows Q for $\beta=0.8°$. For $\Gamma=0$, the flow could jam, but no stable jams were observed in the presence of vibrations. For $\Gamma<1$, the flow was either steady or flow with jams, depending on the initial state of the funnel (unfilled or filled, respectively) as found for an unvibrated flow (see Sec. IV A). For $\Gamma\sim 1-4$, it then becomes solely flow with jams, in which case the flow rate varies wildly due to the large fluctuations in the jam durations. The flow rate stabilizes for $\Gamma>4$ (excited flow) and becomes constant. The final value decreases with increasing A, but it appears to reach a lower bound when $A\sim 6$ mm.

3. $\beta=2.0°,\ 3.1°$

Figure 12(c) shows Q for $\beta=3.1°$. Jams do not occur even for $\Gamma=0$, the flow is steady, and the flow rate is always relatively stable. Beyond $\Gamma\sim 4$, the flow is excited and the flow rate is constant, saturating again when $A\sim 6$ mm.

4. $\beta \geqslant 4.2°$

Figures 12(d) and 12(e) show Q for larger funnel angles. Generally, the flow behavior now only seems to depend on Γ alone, i.e., there is no dependence on A. This region has already been discussed in Sec. VI A. For $\Gamma<1$, there are stable jams. For $\Gamma\sim 1-4$, there is again flow with jams, and again the flow rate fluctuates due to the large variations in jam durations. (It is not understood why flow with jams occurs in two different regions of the phase diagram.) However, note that there appears to be, on average, a curious dip in the flow rate at $\Gamma\sim 2$. For $\Gamma>4$, the flow is excited and the flow rate is constant, at roughly the same value as for smaller β.

C. Flow rates for $D=4$ mm ($D/d=1.68$)

The flow behavior was also studied for larger outlet widths. Even for $D=4$ mm ($D/d=1.68$), jams no longer occurred without vibrations for all measured values of β. The same qualitative behavior was also observed for $D=5$ mm ($D/d=2.10$) and will not be shown.

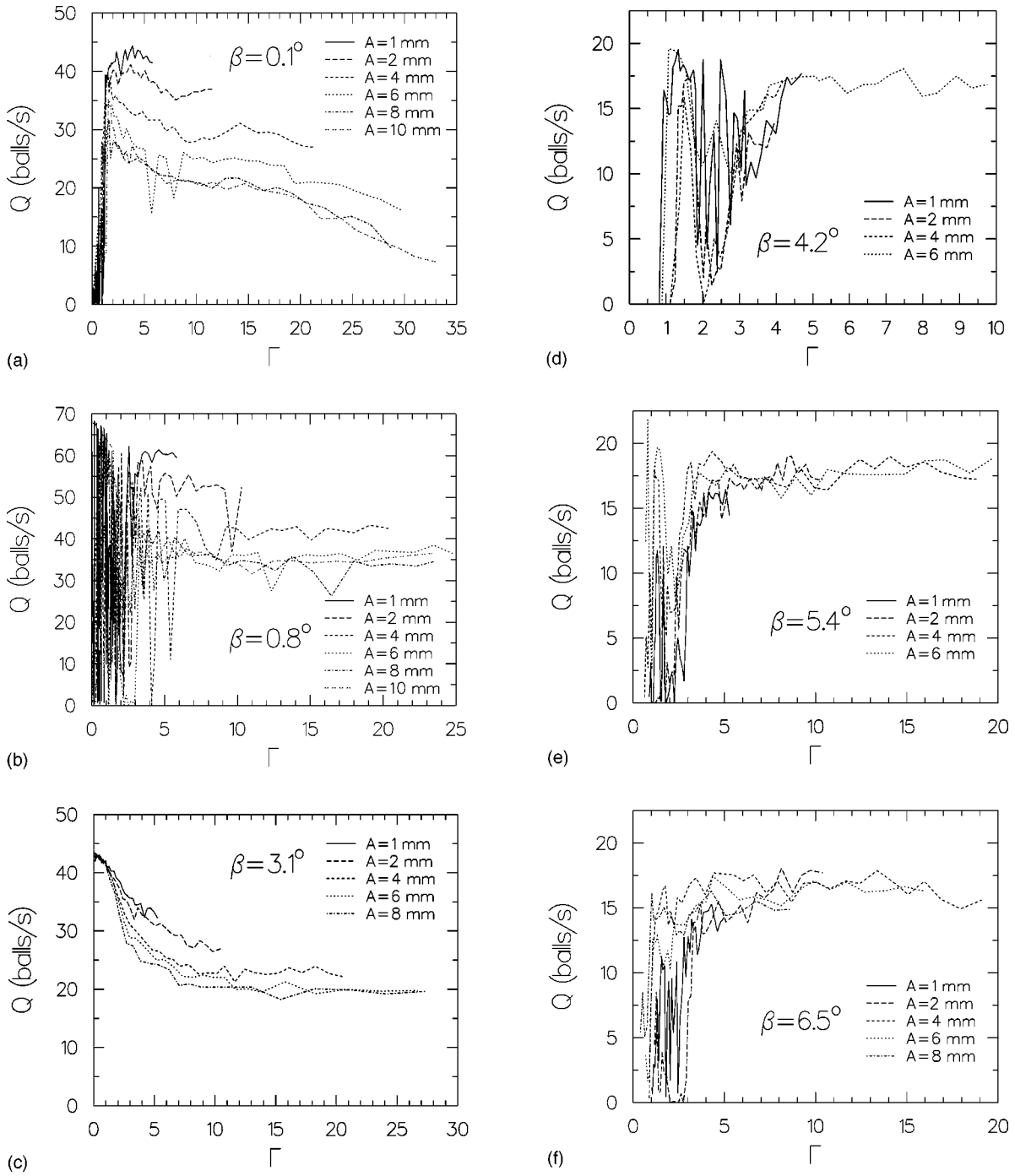

FIG. 12. Flow rates vs Γ with different driving amplitudes for $D=3$ mm ($D/d=1.26$) and different funnel angles: (a) $\beta=0.1°$, (b) $\beta=0.8°$, (c) $\beta=3.1°$, (d) $\beta=4.2°$, (e) $\beta=5.4°$, (f) $\beta=6.5°$.

Flow rate curves for $D=4$ mm are shown in Figs. 13(a) and 13(b). The flow is steady for $\Gamma<1$. However, for $\Gamma \sim 1-3$, jams begin to appear (although too rarely to obtain any reliable statistics) resulting in occasional large fluctuations in the flow rates. It therefore appears that in this case vibrations actually *enhance* the ability to jam, possibly because transverse collisions with the walls disrupt the flow, giving them a chance to form. The flow rate becomes constant beyond $\Gamma \sim 5$, again saturating when $A \sim 6$ mm.

Previous work on vibrated flows examined larger values of both β and D/d than reported here. Wassgren *et al.* [3] have studied the flow in a vertically vibrated vertical wide-angle ($\beta=45°$) hopper for $D/d \sim 3$ and $\Gamma=0-4$ at fixed frequencies between 20 and 60 Hz. They found that with increasing Γ, the flow rate dropped $\sim 20\%$ at 20 Hz, remained constant at 50 Hz, and increased $\sim 10\%$ at 60 Hz. They concluded that the flow rate was not a function of Γ, but of a dimensionless velocity $\Gamma_v \sim A\omega$. However, based on our observations, it may be that they did not study large enough Γ where it may become the relevant variable. (A similar system was subjected to transverse vibrations in which case the flow rate increased up to $\sim 10\%$ with increasing Γ [4].)

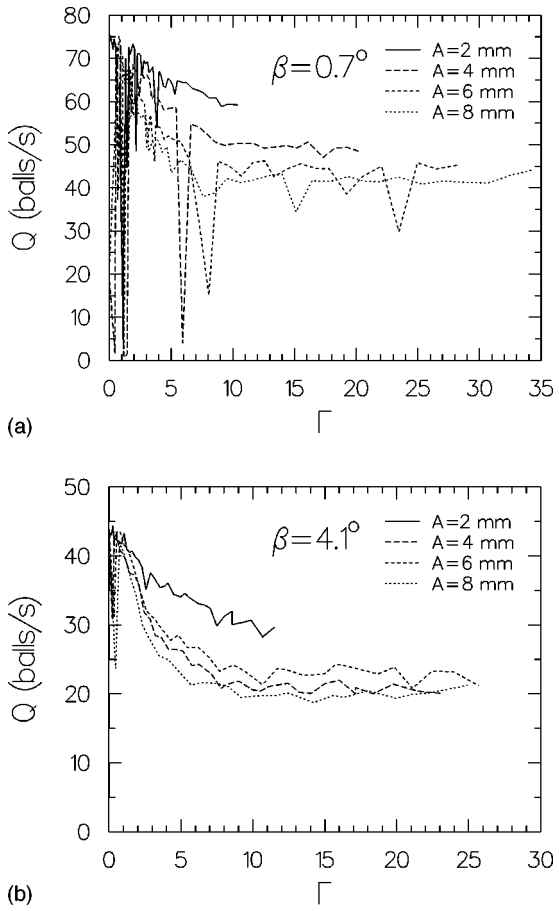

FIG. 13. Flow rates vs Γ with different driving amplitudes for $D=4$ mm ($D/d=1.68$) and different funnel angles: (a) $\beta=0.7°$, (b) $\beta=4.1°$.

Evesque and Meftah [5] have measured flow rates in a vertically vibrated hourglass with $D/d\sim 9$ and $\Gamma=0-5$ at fixed frequencies between 5 and 100 Hz. (No funnel angle was given although it is usually not well-defined for a classic hourglass.) They generally observed that the flow rate decreased significantly with increasing Γ (although in some cases there was first a weak maximum at $\Gamma\sim 0.6$). In particular, the flow stopped completely for $\Gamma>2$ and $40<f<60$ Hz. Such an effect was never observed in our experiments.

D. Elapsed time measurements

We now discuss the analysis of the binary ball function $B(t)$ discussed in Sec. III. It was only measured for $D=3$ mm ($D/d=1.26$), where relatively long-lived jams occurred frequently enough for study.

First, we generate histograms of the elapsed times $N(\sigma)$. In some cases, in order to reveal the tails of these histograms more clearly, we also show the cumulative distribution $N(\sigma'\geqslant\sigma)$, i.e., the number of elapsed times greater than or equal to a given measured elapsed time. The distributions for the blocked time σ_b were, as expected, relatively narrow and are not shown. However, one can use the mean blocked time to obtain the mean ball velocity $v=d/\langle\sigma_b\rangle$. The mean free path is then $\ell=v\langle\sigma\rangle=(\langle\sigma\rangle/\langle\sigma_b\rangle)d$. The mean density is then $n=(\ell+d)^{-1}$ and the mean flow rate is $Q=nv=(\langle\sigma\rangle+\langle\sigma_b\rangle)^{-1}$.

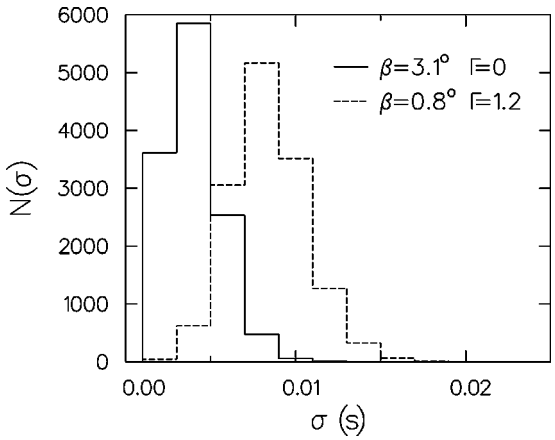

FIG. 14. Histograms of elapsed times for two configurations with steady flow: unvibrated ($\Gamma=0$) and vibrated ($\Gamma=1.2$,$A=6$ mm,$f=1.9$ Hz).

Second, we compute the power spectrum $S(\omega)\sim|\tilde{B}(\omega)|^2$, where $\tilde{B}(\omega)$ is the Fourier transform of $B(t)$. Since only single balls pass through the beam, the power spectrum can be written in the more specific form

$$S(\omega)\sim|\tilde{F}(\omega)|^2\left[1+\frac{1}{N}\sum_{j\neq k}^{N}e^{i\omega(t_j-t_k)}\right], \tag{2}$$

where $\tilde{F}(\omega)=4\sin(\omega\sigma_b/2)/\omega$ is the shape function for a single ball, N is the number of balls, and the sum is over all ball detection times t_j. (The form for the shape function assumes a constant velocity for the balls, although in reality the relatively narrow velocity distribution will smear it. Nevertheless, it will suffice for our purposes.) The first term in the brackets represents the self-correlations, and the sum represents the correlations between different balls. From the power spectrum, we obtain the correlation function $C(\tau)=\langle B(t)B(t+\tau)\rangle$. If $B(t)$ becomes uncorrelated with itself for sufficiently large τ, then $C(\tau)\rightarrow\langle B\rangle^2$. For a binary function, we note that $0<C(\tau)<1$ and

$$\langle B\rangle=\langle B^2\rangle=nd=\frac{1}{1+\ell/d}=\frac{1}{1+\langle\sigma\rangle/\langle\sigma_b\rangle}. \tag{3}$$

1. Steady flow

Histograms of the elapsed times for two different configurations in the steady flow regime (see Fig. 11) are shown in Fig. 14. In both cases, the distributions are relatively narrow and without significant tails. (The largest elapsed time was $\sim$0.07 s.) This suggests a nearly periodic flow. For the unvibrated flow (solid line), we find that $\langle\sigma\rangle\simeq 0.004$ s and $\langle\sigma_b\rangle\simeq 0.020$ s, hence $\langle B\rangle\simeq 0.83$. Therefore, $v\sim 12$ cm/s, $\ell\sim 0.2d\sim 0.5$ mm, and $Q\sim 42$ balls/s [cf. Fig. 12(c)].

For the vibrated flow (dashed line), the entire distribution broadens slightly and shifts to longer times, indicating that the balls are either moving slower or the mean free path has increased. We now find $\langle\sigma\rangle\simeq 0.008$ s and $\langle\sigma_b\rangle\simeq 0.013$ s, hence $\langle B\rangle\simeq 0.62$. Thus, $v\sim 18$ cm/s,$\ell\sim 0.6d\sim 1.5$ mm, and $Q\sim 48$ balls/s. Thus, the balls are moving *faster* by 50% for a vibrated flow, but the mean path path has increased by

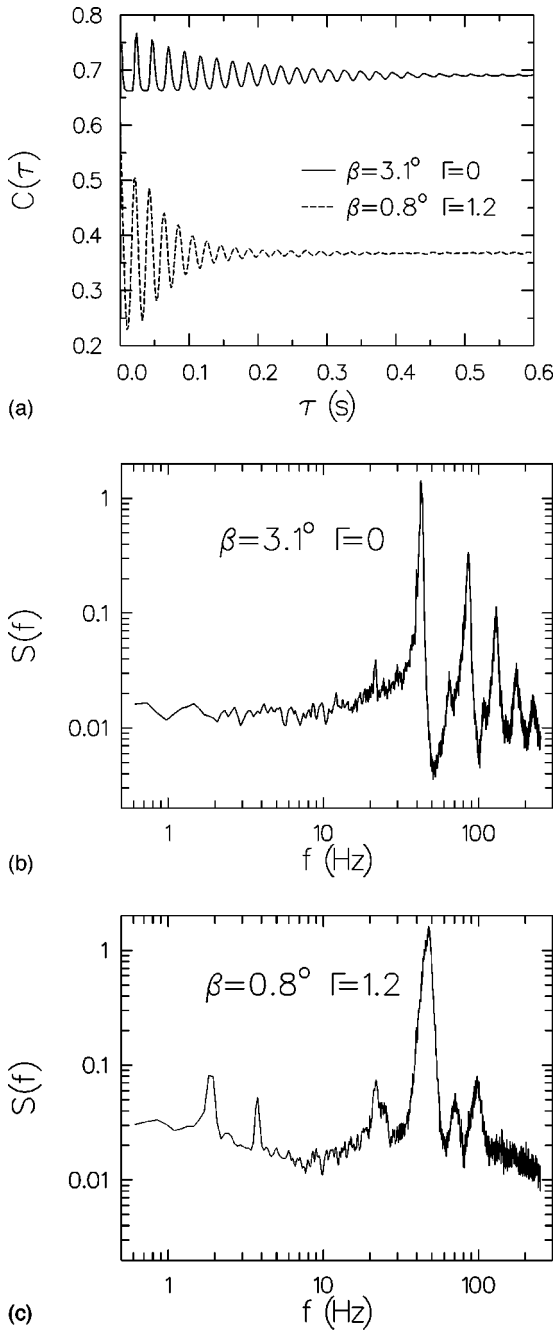

FIG. 15. (a) Correlation function for an unvibrated (solid line) and vibrated (dashed line) system in a regime with steady flow (see text). Only the first 0.6 s are shown. (b) Averaged power spectrum of the unvibrated data in (a). The periodic flow of the balls is visible as a peak at ~ 42 Hz and its harmonics. (c) Averaged power spectrum of the vibrated data in (a). The flow is still nearly periodic, but there are now stronger subharmonic structures (see text). The peaks at 1.9 Hz and 3.8 Hz are the vibration frequency and its second harmonic. (Both spectra are flat below 1 Hz and are not shown in order to see the details at higher frequency.)

300%. Interestingly, the end result is that the flow rate has actually increased slightly.

In Fig. 15(a), the first 0.6 s of $C(\tau)$ is shown (solid line) for the unvibrated data set in Fig. 14. The oscillations confirm that the signal is nearly periodic, i.e., individual balls are leaving the funnel at well-defined intervals $T \sim 0.025$ s $\sim Q^{-1}$. As expected, $B(t)$ becomes uncorrelated for long times, and $C(\tau) \rightarrow \langle B \rangle^2 \simeq 0.69$, which is consistent with the value obtained above. The envelope is essentially exponential, i.e., $C(\tau) \sim e^{-\tau/\tau_0}$ and the coherence time is $\tau_0 \sim 0.15$ s. The same information is contained in the power spectrum shown in Fig. 15(b). There is a peak at ~ 42 Hz, which is just the inverse of the period T, and which has a width corresponding to the inverse of the coherence time. One also observes its harmonics at higher frequencies.

One can also obtain the velocity from the zeros $f_n = \omega_n/2\pi = nv/d$ for integer n of the shape function $\tilde{F}(\omega)$. Since $\sigma_b \lesssim T$, these can be seen at slightly higher frequencies than the peaks (although, due to smearing, they are not true zeros). The first zero at ~ 50 Hz again yields $v \sim 12$ cm/s.

The subharmonic at ~ 22 Hz indicates that the symmetry of the periodic flow is, in fact, weakly broken, resulting in a period doubling. This could, for example, be due to a weak pairing of the balls, but is more likely due to the fact that the balls tend to leave the funnel alternately from the left and right walls, and that these balls are detected slightly differently by the optical system.

When the system is vibrated, the results are qualitatively the same but with some quantitative differences. The correlation function in Fig. 15(a) (dashed line) shows a slightly faster periodicity of the balls $T \sim 0.02$ s. It now converges to $\langle B \rangle^2 \simeq 0.37$, consistent with the value obtained earlier and the now lower density [or longer mean free path; see Eq. (3)]. The coherence time has now decreased to $\tau_0 \sim 0.08$ s. Thus, not surprisingly, even relatively weak vibrations disturb the periodicity.

The corresponding power spectrum is shown in Fig. 15(c). The main peak now occurs at $T^{-1} \sim 48$ Hz and is noticeably broader than the peak in Fig. 15(b) due to the shorter coherence time. The subharmonic peaks are now also noticeably stronger, indicating a greater asymmetry in the way the balls leave the funnel. The zeros of the shape function are now too smeared to be obvious, but the first should now occur at $f_1 = v/d = \langle \sigma_b \rangle^{-1} \sim 77$ Hz where there is, in fact, a minimum.

The peak at 1.9 Hz is just the vibration frequency. (Its second harmonic at 3.8 Hz is also visible.) Apparently, there are correlations at the vibration frequency as well. Since we can see no obvious modulation of $B(t)$ at this frequency, it may be, for example, that a ball is almost always ejected (or not ejected) at the same point in the vibration cycle, probably when the displacement is a maximum. The general sharpness of these vibration peaks, and the presence of their harmonics, supports this hypothesis.

2. Flow with jams

Figure 16(a) shows histograms of the elapsed times for three different configurations in regimes with flow with jams. All three appear to have roughly exponential tails. (If the elapsed times were random, their distribution would be purely exponential.) However, the distribution for $\beta = 6.5°$, $A = 2$ mm does not have a distinct sharp peak at very small σ as do the other two. Moreover, the distribution for $\beta = 0.8°$ has a decay time of ~ 0.003 s whereas both distributions for $\beta = 6.5°$ have decay times of ~ 0.02 s. Thus, although all three flows are termed ''flow with jams'' follow-

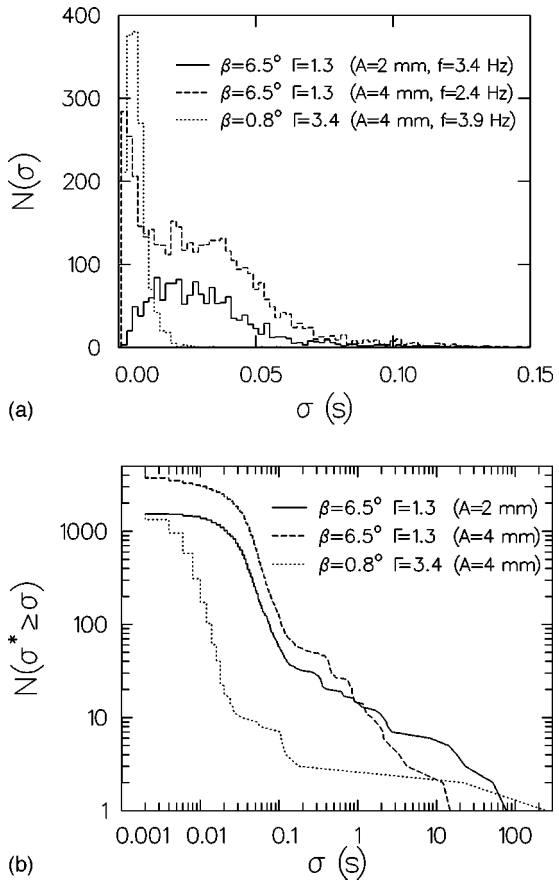

FIG. 16. (a) Histograms of elapsed times for three configurations which exhibit flow with jams. Only the first 0.15 s are shown. (b) Cumulative distributions of the same data. (Lines are drawn for clarity.)

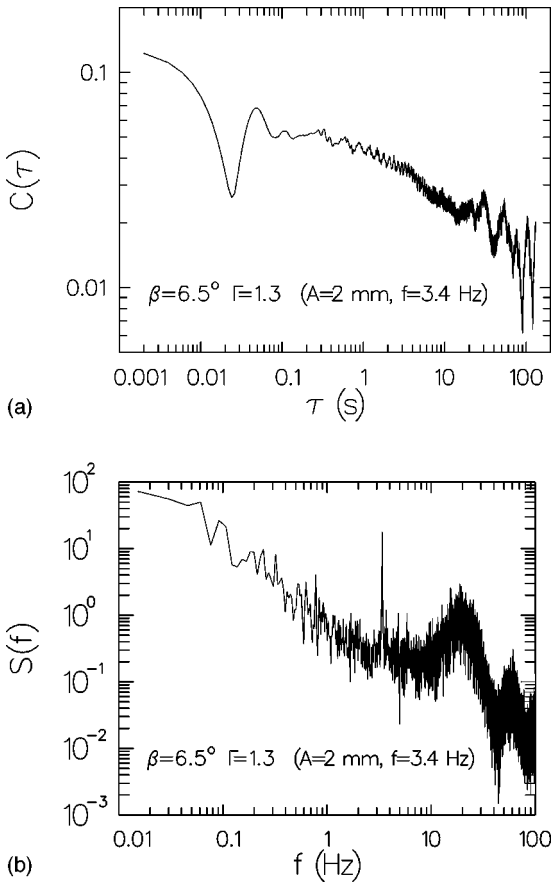

FIG. 17. (a) Correlation function for the first configuration (solid line) in Fig. 16(b). (b) Averaged power spectrum for the configuration in (a). (It has been truncated at 100 Hz for clarity.) The vibration frequency appears as a peak at 3.4 Hz. The broad peak at ~20 Hz is due to the weak periodicity induced by the hard-sphere excluded region (see text).

ing their observed behavior (see Fig. 11), nevertheless qualitative differences exist between them depending on the precise values of β and Γ.

The cumulative distributions of the data in Fig. 16(a) are shown in Fig. 16(b). For $\sigma > 0.1$ s, one can now see the long tails of the distributions due to jams which last as long as ~200 s (approximately 800 vibrations of the system). These tails certainly decay slower than exponentially, and are perhaps algebraic, but the statistics are too poor to be convincing. (In any case, the exponent would certainly be rather different for the three distributions.) Thus, there appear to be two temporal regions: a short one with exponential behavior resulting from the periods of flow, and a longer one, possibly algebraic, from the jams. In particular, both distributions for $\beta = 6.5°$ have relatively many long jams, whereas that for $\beta = 0.8°$ has only two that exceed 1 s. Thus, reasonably, the jams for $\beta = 6.5°$ are measureably more stable than those for $\beta = 0.8°$.

We will now focus on the first of the distributions in Figs. 16(a) and 16(b) (solid lines), which had the longest jams. First, we find that $\langle \sigma \rangle \simeq 0.17$ s and $\langle \sigma_b \rangle \simeq 0.023$ s, hence $\langle B \rangle \simeq 0.12$. Therefore, $v \sim 10$ cm/s, $\ell \sim 7.4d \sim 1.8$ cm, and $Q \sim 5$ balls/s [roughly the mean in Fig. 12(f)]. Obviously, the mean free path has increased due to the jams. The velocity of the balls (when they are flowing) is not significantly different from that for steady unvibrated flow.

The correlation function $C(\tau)$ is shown in Fig. 17(a) on a log-log plot to capture a wider range of time scales. The minimum at $\tau \sim 0.024$ s corresponds to the excluded region of hard spheres during periods of flow and is, not surprisingly, approximately the blocking time σ_b. It is followed by a weak peak at twice the minimum time (i.e., $\tau \sim 0.048$ s) corresponding to the increased likelihood of finding two balls together. The rise to the left of the minimum is from self-correlations. The small regular oscillations around $\tau \sim 2$ s correspond to the vibration frequency, *not* to any periodic flow of the balls. The large irregular oscillations for $\tau > 10$ s are due to the longest jams. The overall decay is not well-defined in any sense, and $C(\tau)$ does not approach its uncorrelated value $\langle B^2 \rangle \simeq 0.014$ in a direct manner, indicating that there are still correlations.

The corresponding power spectrum shown in Fig. 17(b) is more revealing. The peak at 3.4 Hz is just the vibration frequency again. The broad peak at ~20 Hz is due to the very weak periodicity created by the hard-sphere exclusion during flow, and corresponds to the inverse of the weak peak to the right of the minimum in the correlation function. One also expects this to occur at a frequency corresponding to the most likely time interval between balls, namely, the blocking time σ_b plus the location of the peak in the distribution shown in Fig. 16(a), which is ~0.025 s. Hence, the peak

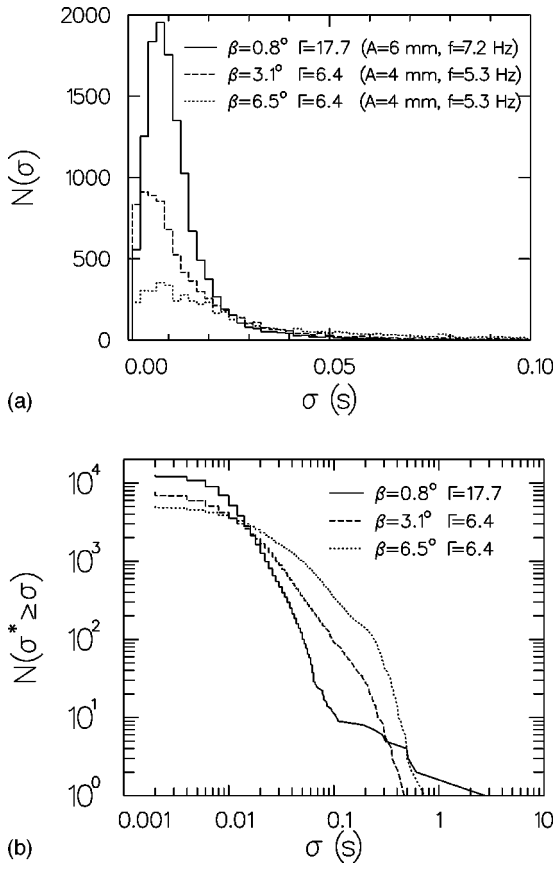

FIG. 18. (a) Histograms of the elapsed times for three configurations exhibiting excited flow. Only the first 0.1 s is shown. (b) Cumulative distributions of the same data. (Lines are drawn for clarity.)

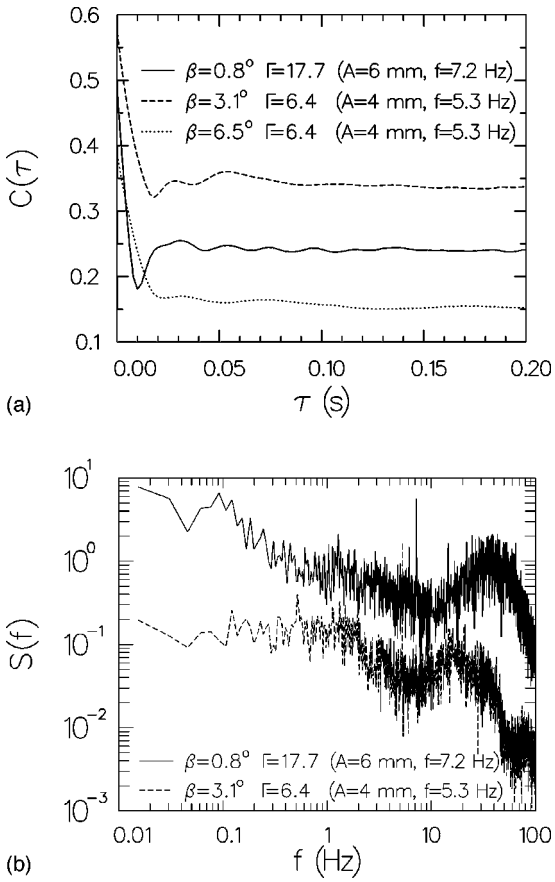

FIG. 19. (a) Correlation functions of the configurations in Fig. 18. Only the first 0.2 s is shown. (b) Averaged power spectra for the first two configurations in (a) (see text). (They have been truncated at 100 Hz for clarity.)

should occur at $(0.025+0.023)^{-1}\sim 20$ Hz. (This should also be the flow rate Q during periods of flow.) The width of this peak therefore gives an estimate of the coherence time of flowing balls. It is ~ 0.03 s, which is only slightly longer than the blocking time, hence the spacing is probably random beyond the hard-sphere excluded region. The oscillations at yet higher frequency are not harmonics of any periodicity, but are almost entirely due to the passing of almost uncorrelated individual balls. Thus, this is just the shape function itself [see Eq. (2)]. As before, from the first zero of the shape function at ~ 40 Hz, one extracts an average ball velocity $v\sim 10$ cm/s, consistent with the earlier result.

Finally, unlike the previous spectra shown in Figs. 15(b) and 15(c), the spectrum in Fig. 17(b) is not white at frequencies below ~ 1 Hz. (The power spectra for the other two configurations in Fig. 16 were qualitatively similar.) This is not surprising given the presence of long-lived jams. In particular, the nonwhite behavior in the frequency range 0.01–1 Hz corresponds to the long jam times of 1–100 s observed in Fig. 16(b). [If one wishes to play the exponent game, then in this regime $S(\omega)\sim\omega^{-1.3}$, so this may be an example of so-called $1/f$ noise.] If there are indeed long-time correlations, however, we have no explanation as to their origin.

3. Excited flow

Figure 18(a) shows the elapsed time histograms for three different configurations exhibiting excited flow. They all have the same qualitative behavior, namely, a peak at ~ 0.01 s and approximately exponential tails with time constants of 0.01–0.03 s. In these respects, these distributions resemble those for flow with jams [cf. Fig. 16(a)].

In particular, for the first distribution in Fig. 18(a) (solid line), which is the most excited (largest value of Γ), we find that $\langle\sigma\rangle\simeq 0.012$ s, $\langle\sigma_b\rangle\simeq 0.012$ s, and $\langle B\rangle\simeq 0.49$. Therefore, $v\sim 20$ cm/s, $\ell\sim d\sim 2.4$ mm, and $Q\sim 42$ balls/s [cf. Fig. 12(b)]. The velocity of the balls as they leave the funnel is generally higher than for steady flow or flow with jams.

For the second distribution in Fig. 18(a) (dashed line), we find that $\langle\sigma\rangle\simeq 0.017$ s, $\langle\sigma_b\rangle\simeq 0.022$ s, and $\langle B\rangle\simeq 0.58$. Therefore, $v\sim 11$ cm/s, $\ell\sim 0.8d\sim 1.8$ mm, and $Q\sim 26$ balls/s [cf. Fig. 12(c)]. The velocity here is comparable to the other flow regimes.

For the third distribution in Fig. 18(a) (dotted line), we find that $\langle\sigma\rangle\simeq 0.037$ s, $\langle\sigma_b\rangle\simeq 0.023$ s, and $\langle B\rangle\simeq 0.39$. Therefore, $v\sim 10$ cm/s, $\ell\sim 1.6d\sim 3.8$ mm, and $Q\sim 17$ balls/s [cf. Fig. 12(f)]. Although the velocity is the same as the previous distribution, the density is distinctly lower.

The cumulative distributions are shown in Fig. 18(b). Only the first configuration (solid line), which is the most excited, has an obvious nonexponential tail, although even it has no elapsed times longer than ~ 3 s. In this case, however, the tail is not due to jams, but to the fact that the balls are violently bouncing around inside the funnel and cannot escape. However, when they do escape, the sharpness of the

distributions in Fig. 18(a) implies that during periods of flow the balls are fairly close together, i.e., they exit the funnel in clusters with relatively high velocities. The first configuration, in particular, shows this effect most dramatically.

The correlation functions are shown in Fig. 19(a). The balls are uncorrelated except for the hard-sphere exclusion at very short times. It is not visible in the third configuration (dotted line) because $\ell/d \sim 1.6$ so the balls have less hard contact than in the first two configurations where $\ell/d \lesssim 1$.

The averaged power spectra for the first two configurations in Fig. 19(a) are shown in Fig. 19(b). The vibration frequencies are just visible at 7.2 Hz and 5.3 Hz, respectively. The broad peaks at ~ 40 Hz and ~ 25 Hz are again due to the weak periodicity induced by the hard-sphere exclusion as already described for the power spectrum for flow with jams in Fig. 17(b). In particular, we note that the nonexponential tail in the cumulative distribution [Fig. 18(b)] for the first configuration (solid line) between 0.1 and 3 s clearly leads to nonwhite behavior in its power spectrum in the corresponding frequency range 0.1–10 Hz. (The unaveraged spectrum, which had a bandwidth of ~ 0.003 Hz, appeared to be white below ~ 0.1 Hz, although the fluctuations were rather large.) By comparison, the second configuration in Fig. 18(b) (dashed line), which had no such tail, has a white spectrum below ~ 1 Hz.

VII. SUMMARY

In this work, we have studied the effect of vibrations on a two-dimensional granular flow in a small-angle funnel. Generally, the most interesting effects occurred for small outlet widths where, without vibrations, the flow simply jammed. Hence, vibrations had the effect of breaking jams. However, in the flow with jams regime, the jams may have relatively long lifetimes. In some cases, this was apparent in the elapsed time distributions with their long, possibly algebraic tails, and also in the corresponding correlation functions and power spectra. In this regime, vibrations also resulted in large fluctuations in flow rates, although they always became stable and constant as Γ was increased, and approached a lower bound for sufficiently large vibration amplitudes. For larger outlet widths ($D = 4$ mm and $D = 5$ mm), there were no jams, and the flow behavior was not nearly as rich. Generally, the flow rate simply decreased $\sim 50\%$ as Γ was increased.

ACKNOWLEDGMENTS

It is a pleasure to thank S. Hørlück and C. Veje for their helpful comments and assistance. P.D. would like to thank Statens Naturvidenskabelige Forskningsråd (Danish Research Council) for support.

[1] C.T. Veje and P. Dimon, Phys. Rev. E **54**, 4329 (1996); C.T. Veje, Master's thesis, University of Copenhagen (1995).
[2] K. Lindemann, Master's thesis, University of Copenhagen (1998).
[3] C.R. Wassgren, M.L. Hunt, and C.E. Brennen, (unpublished).
[4] M.L. Hunt, R.C. Weathers, A.T. Lee, C.E. Brennen, and C.R. Wassgren, Phys. Fluids **11**, 68 (1999).
[5] P. Evesque and W. Meftah, Int. J. Mod. Phys. B **7**, 1799 (1993).
[6] S. Hørlück and P. Dimon, Phys. Rev. E **60**, 671 (1999); S. Hørlück, Master's thesis, University of Copenhagen (1997).
[7] R.L. Brown, Nature (London) **191**, 458 (1961).
[8] R.L. Brown and J.C. Richards, *Principles of Powder Mechanics* (Pergamon Press, Oxford, 1970).
[9] There is an error in the numerical prefactor in Eq. (5) in VD (Ref. [1]).
[10] See, for example, H.M. Jaeger, S.R. Nagel, and R.P. Behringer, Rev. Mod. Phys. **68**, 1259 (1996).